Simulation of temperature and magnetic field distribution in superconducting bulk during pulsed field magnetization

2010 Supercond. Sci. Technol. 23 105021

(http://iopscience.iop.org/0953-2048/23/10/105021)

Supercond. Sci. Technol. **23** (2010) 105021 (8pp) doi:10.1088/0953-2048/23/10/105021

Simulation of temperature and magnetic field distribution in superconducting bulk during pulsed field magnetization

Hiroyuki Fujishiro and Tomoyuki Naito

Faculty of Engineering, Iwate University, 4-3-5 Ueda, Morioka 020-8551, Japan

E-mail: fujishiro@iwate-u.ac.jp

Received 4 July 2010, in final form 3 September 2010
Published 17 September 2010
Online at stacks.iop.org/SUST/23/105021

Abstract

A theoretical simulation of electromagnetic and thermal fields was performed for a cryocooled superconducting bulk disc after applying a magnetic pulse. The results of the simulation qualitatively reproduced the experimental ones for the time and applied field dependences of the trapped field B_z and the temperature T on the bulk surface. For magnetic pulse application with a rise time of $\tau = 0.01$ s, the magnetic flux propagation was about two orders of magnitude faster than the heat propagation because of the low thermal conductivity of the bulk. The results show that the intruding magnetic flux escaped because of the delayed temperature rise. For a longer magnetic pulse application with $\tau = 1$ or 10 s, the flux propagation speed becomes slow and approaches the heat propagation speed. In this case, the magnetic flux escape attributable to the flux creep becomes small and a higher trapped field can be achieved. The method of exploring the enhancement of the trapped field using pulsed field magnetization is discussed.

1. Introduction

Recently, pulsed field magnetization (PFM) for REBaCuO bulk (RE: rare earth element or Y) has been investigated intensively for practical applications as a substitute for field-cooled magnetization (FCM) because PFM is an inexpensive and mobile experimental set-up with no need for a superconducting magnet. The trapped field B_z achievable by PFM is nonetheless lower than that achievable by FCM because of the large temperature rise caused by the dynamical motion of the magnetic flux. Several approaches have been performed and have succeeded in enhancing B_z including an iteratively magnetizing pulsed field method with reducing amplitude (IMRA) [1] and a multi-pulse technique with step-wise cooling (MPSC) [2]. We have experimentally examined the time and spatial dependences of the temperature $T(t, x)$, local field $B_z(t, x)$, and the trapped field B_z on the surface of cryocooled REBaCuO bulks during PFM for various starting temperatures T_s and applied fields B_{ex} [3–5]. To enhance B_z, it is believed that the reduction in temperature rise ΔT and the lowering of T_s are effective because of the enhancement of the critical current density J_c, similar to the case for FCM. Considering the obtained experimental results, we proposed a new PFM technique named modified MPSC (MMPSC) [6] and successfully realized a highest field trap of $B_z = 5.20$ T on a ⌀45 mm GdBaCuO bulk at 30 K [7], which is a record-high value by PFM to date. However, experimental research has been limited. Results have shown little progress to explore the enhancement of the trapped field using PFM. It is necessary to use a theoretical simulation to elucidate the multi-physics in the bulk during PFM.

Several studies of theoretical simulations for PFM have been reported. Many of the studies were performed under conditions in which the bulk was immersed in liquid nitrogen. Simulations have been performed also for cryocooled bulks; Kajikawa *et al* reported theoretical results of the MMPSC method, in which the experimental results were reproduced qualitatively through the simulation [8]. Komi *et al* reported magnetic and thermal fields during PFM in a cryocooled bulk with inhomogeneous superconducting properties [9]. We investigated heat propagation in drilled holes in the bulk both experimentally [10] and theoretically [11]. The results suggest that the heat generation took place adiabatically because of its greater heat generation than the cooling power of the refrigerator.

As described in this paper, we constructed the framework of the theoretical simulation in the superconducting bulk with

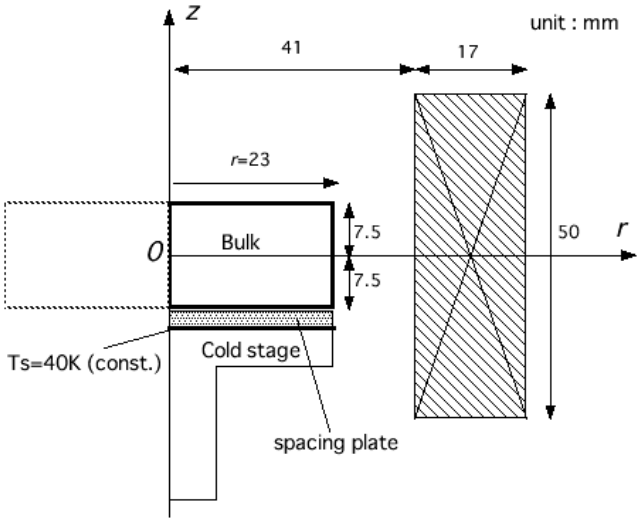

Figure 1. Structure and dimensions around the bulk and solenoid copper coil for pulsed field magnetization (PFM). The 1 mm thick spacing plate with thermal conductivity of κ_{cont} was placed between the bulk and the cold stage of the refrigerator, which imaginarily represents the cooling power of the refrigerator and the thermal contact of the bulk on the cold stage.

homogeneous superconducting properties after a magnetic pulse application using the finite element method (FEM). We reproduced the experimental results using the simulation. We also investigated the effect of a magnetic pulse application with a longer rise time of $\tau = 1$ or 10 s on the $B_z(t)$ and $T(t)$ values than those using a magnetic pulse with $\tau = 0.01$ s, which was used experimentally because the long pulse application enhanced the trapped field experimentally [12]. The direction to explore the enhancement of the trapped field by PFM is discussed herein.

2. Modelling and theoretical simulation

Based on our experimental set-up around the bulk [5], the framework of the theoretical simulation was constructed. A schematic view is presented in figure 1. A superconducting bulk disc of 46 mm diameter and 15 mm thickness was stacked on the cold stage of a refrigerator in a vacuum chamber and cooled to the starting temperature $T_s = 40$ K. We set the spacing plate with thermal conductivity κ_{cont} between the bulk and the cold stage to 1 mm thickness, which imaginarily represents both the cooling power of the refrigerator and the thermal contact. Then κ_{cont} was set as 0.5 W mK^{-1} based on the experimental results of $T(t)$ on the bulk surface [6]. In the simulation, the bulk was magnetized using a solenoid-type copper coil (82 mm I.D., 116 mm O.D., and 50 mm height). Physical phenomena during PFM are described using electromagnetic and thermal fields. The equations and parameters were taken from [9]. Commercial software, Photo-Eddy, combined with Photo-Thermo (Photon Ltd, Japan), was used for analyses of the magnetic field and temperature distribution in superconducting bulk during PFM.

Their fundamental equations on the axisymmetric coordinate are as follows.

$$\frac{\partial}{\partial r}\left[\frac{\nu}{r}\frac{\partial}{\partial r}(rA)\right] + \frac{\partial}{\partial z}\left(\nu\frac{\partial A}{\partial z}\right) = J_0 + J \tag{1}$$

$$\rho C\frac{\partial T}{\partial t} = \frac{1}{r}\frac{\partial}{\partial r}\left(r\kappa_{ab}\frac{\partial T}{\partial r}\right) + \frac{\partial}{\partial z}\left(\kappa_c\frac{\partial T}{\partial z}\right) + Q. \tag{2}$$

Therein, A represents the magnetic vector potential, J_0 is the forced current density or coil current density, J denotes the superconducting current density or induced current density, and Q signifies the heat generation. In equation (2), T denotes the temperature, C is the specific heat, and κ_{ab} and κ_c respectively denote the thermal conductivity in the ab-plane and along the c-axis.

The J value is given as

$$J = \sigma E = -\sigma\frac{\partial A}{\partial t}, \tag{3}$$

where E is the electric field and σ is the electrical conductivity. Then FEM analysis of the coupled problem with electromagnetic field and heat diffusion was performed.

The power-n model was used to describe the nonlinear E–J characteristic in superconducting bulk, as

$$E = E_c\left(\frac{J}{J_c}\right)^n, \tag{4}$$

where J_c is the critical current density and E_c is the reference electric field. The magnetic field dependence of the J_{c0} was described using the Kim model [13] as

$$J_c = J_{c0}\frac{B_0}{|B| + B_0}, \tag{5}$$

where J_{c0} is J_c for $B = 0$ and B_0 is constant. The temperature dependence of J_{c0} is described by the following equation,

$$J_{c0} = \alpha\left\{1 - \left(\frac{T}{T_c}\right)^2\right\}^{\frac{3}{2}}, \tag{6}$$

where T_c is the critical temperature (=92 K) at $B = 0$ and α is constant. Heat generation Q in the conductor is given as $Q = JE$. Iterative calculations were performed to obtain the convergence of σ in the superconductor at each time step.

The applied pulsed field $B_{ex}(t)$ with the rise time of $\tau = 0.01$ s was approximated in the following equation:

$$B_{ex}(t) = B_{ex}\frac{t}{\tau}\exp\left(1 - \frac{t}{\tau}\right). \tag{7}$$

The numerical values for the parameters used in the simulation are presented in table 1. The κ_{ab}, κ_c and C values were presumed to be temperature-independent for simplicity.

3. Example of experimental results

Let us show an example of the experimental results of the trapped field on the bulk magnetized by PFM. Figure 2(a)

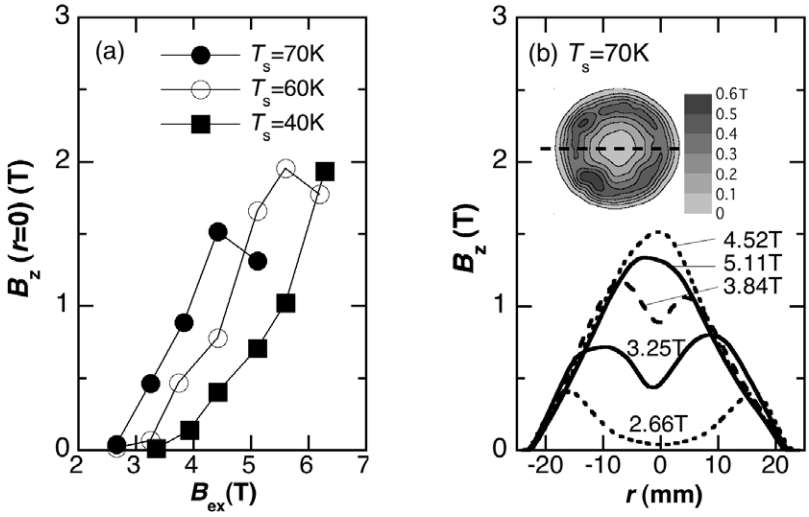

Figure 2. Example of experimental results for the trapped field on the GdBaCuO bulk magnetized by PFM [4]. (a) Trapped field $B_z(r = 0)$ at the centre of the bulk at various starting temperatures T_s after applying a pulsed field B_{ex} with a rise time of $\tau = 0.01$ s. (b) Cross-section of the B_z profiles for various applied pulsed fields B_{ex} at $T_s = 70$ K. In the inset, an example of the two-dimensional B_z profile is shown for $B_{ex} = 2.66$ T.

Table 1. Numerical values for parameters used in the simulation.

Symbol	Parameter	Value
T_c	Transition temperature in equation (6)	92 K
ρ	Mass density of bulk in equation (2)	5.9×10^3 kg m^{-3}
C	Specific heat of bulk in equation (2)	1.32×10^2 J kg^{-1} K^{-1}
κ_{ab}	Thermal conductivity of bulk along the *ab*-plane in equation (2)	20 W mK^{-1}
κ_c	Thermal conductivity of bulk along the *c*-axis in equation (2)	4 W mK^{-1}
n	*n*-value in equation (4)	8
E_c	Constant in equation (4)	1×10^{-6} V m^{-1}
B_0	Constant in equation (5)	1.3 T
α	Constant in equation (6)	0.23–1.83×10^9 A m^{-2}
σ	Electrical conductivity ($T > T_c$) in equation (3)	1×10^3 S cm^{-1}
τ	Rise time of the pulse in equation (7)	0.01, 1, 10 s
κ_{cont}	Thermal conductivity of spacing plate	0.5 W mK^{-1}

shows the trapped field $B_z(r = 0)$ at the centre of the GdBaCuO bulk (45 mm in diameter and 18 mm in thickness) after applying a pulsed field B_{ex} at various starting temperatures T_s [4]. The rise time τ of the pulsed field was 0.01 s. $B_z(r = 0)$ at $T_s = 70$ K starts to increase for $B_{ex} \geqslant 2.7$ T, takes a maximum at $B_{ex} = 4.4$ T and then decreases with increasing B_{ex}. For lower T_s, the applied field, at which the magnetic flux starts to be trapped at the bulk centre, and the peak of the $B_z(r = 0)$ value increase with decreasing T_s because of the enhancement of the critical current density J_c.

Figure 2(b) presents a vertical cross-section of the $B_z(r)$ profiles after applying a pulsed field at $T_s = 70$ K [4]. In the inset, an example of the two-dimensional B_z profile is shown for $B_{ex} = 2.66$ T. The trapped field profile changes from a concave shape for $B_{ex} \leqslant 3.84$ T to a convex shape for $B_{ex} \geqslant 4.52$ T. For lower $T_s = 40$ K, similar changes of the B_z profile were observed as a function of B_{ex} (not shown). However, $B_z(r = 0)$ at the bulk centre was small, even if a pulsed field with identical strength was applied as that at 70 K. The maximum $B_z(r = 0)$ increases to 1.8 T for $B_{ex} = 6.29$ T, but the convex profile cannot be realized because of the strong pinning force at low temperatures.

4. Results of simulation and discussion

4.1. Applied field dependence of trapped field

Figure 3(a) depicts the results of the simulation of the trapped field $B_z(r = 0)$ at the centre of the bulk surface as a function of the applied field B_{ex} for various α values in equation (6). The J_{c0} values at 40 K for $\alpha = 1.83 \times 10^9$, 9.2×10^8, 4.6×10^8 and 2.3×10^8 are, respectively, $J_{c0} = 1.33 \times 10^9$, 6.6×10^8, 3.3×10^8 and 1.6×10^8 A m^{-2}. The J_{c0} values for a typical superconducting bulk are, respectively, 2–3 $\times 10^9$ A m^{-2} at 40 K and 1–2 $\times 10^8$ A m^{-2} at 77 K [14]. Therefore, $\alpha = 1.83 \times 10^9$ is a typical value of the bulk at 40 K. In all cases, the $B_z(r = 0)$ starts to increase concomitantly with increasing applied pulsed field B_{ex}, becomes maximum and then decreases with a further increase in B_{ex}. The critical applied field B_{ex}^C, at which the magnetic flux starts to trap at the bulk centre, increases concomitantly with increasing α. The results presented in figure 3(a) can also be interpreted as the T_s dependence of $B_z(r = 0)$ for various B_{ex} for the bulk with constant α, which is consistent with the experimental results shown in figure 2(a). Although the trapped field B_z^{FC} achieved by FCM increases concomitantly with increasing J_c, the trapped field B_z achieved by PFM is not necessarily enhanced for higher J_c because of the large temperature rise, as described in section 4.2.

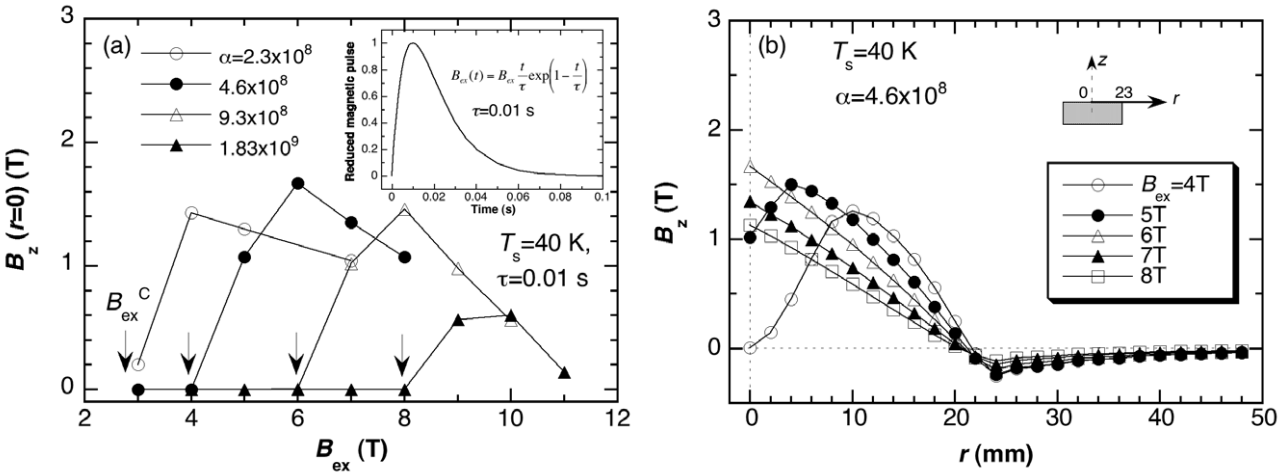

Figure 3. (a) Results of simulation of applied field dependence of the trapped field B_z at the bulk centre ($r = 0$) for various α values ($T_s = 40$ K). The inset shows the time dependence of the normalized magnetic pulse. Arrows indicate the critical applied field B_{ex}^{C} for each α value (see the text). (b) Cross-section of the trapped field profiles for $\alpha = 4.6 \times 10^8$ at $T_s = 40$ K as a function of B_{ex} (simulation).

In the simulation, the maximum temperature $T_{max}(r = 0)$ at the centre of the bulk surface increased concomitantly with increasing B_{ex}, which was independent of the α value. These results suggest that the generated heat was determined by the strength of B_{ex} and that the temperature rises adiabatically because of the smaller heat transfer to the cold stage. The result reproduces the experimental results, in which T_{max} for the YBaCuO bulk with a lower pinning force is nearly the same as that for the GdBaCuO bulk with a higher pinning force [5].

Figure 3(b) presents a cross-section of the trapped field $B_z(r)$ profile for $\alpha = 4.6 \times 10^8$ for various applied fields B_{ex}. The positions of $r = 0$ and 23 mm are, respectively, the centre and edge on the bulk surface. The $B_z(r)$ profile changes from concave for lower B_{ex} to convex for higher B_{ex} and then the $B_z(r = 0)$ value decreases with further increases in B_{ex}. These behaviours are apparent for each α value and are consistent with the experimental ones as shown in figure 2(b). In this way, the results of the numerical simulation reproduced the experimental ones qualitatively.

4.2. Time dependence of local field and temperature

Figures 4(a) and (b) respectively show the time evolution and spatial distribution of the local magnetic field $B_z(t, r)$ and the temperature $T(t, r)$ on the bulk surface after applying a pulsed field of $B_{ex} = 6$ T for $\alpha = 4.6 \times 10^8$ ($J_{c0} = 3.3 \times 10^8$ A m^{-2}). The left and right parts of each figure respectively show ascending ($t \leqslant 0.01$ s) and descending ($t \geqslant 0.01$ s) stages. For the ascending stage, the magnetic flux intrudes gradually into the bulk from the bulk periphery and the magnetic gradient increases with approach to the bulk centre at $t = 0.01$ s. It should be noted that the magnetic flux concentration took place outside the bulk because of the diamagnetism of superconducting bulk, and that a magnetic field of 6.8 T was applied along the z-axis at $r = 23$ mm. For the descending stage ($t \geqslant 0.01$ s), the magnetic field decreased gradually at the outer region with increasing time. On the other hand, the local field near the bulk centre increases to 3 T at $t = 0.1$ s and then decreases gradually to $B_z = 1.7$ T at the steady state.

In figure 4(b), the temperature $T(t)$ at the bulk periphery increases gradually with time at the ascending stage, e.g. $T = 78$ K at $t = 0.01$ s. However, the temperature for $r = 0$ remains as 40 K. At the descending stage, the generated heat diffuses to the bulk centre gradually. In line with the isothermal temperature profile along the r-direction at $t = 5$ s, the temperature decreases concomitantly with increasing time. In this case, a temperature gradient exists along the z-direction because the bottom of the spacing plate was fixed at 40 K.

Figures 5(a) and (b) show the time dependence of local fields $B(r, t)$ and the temperatures $T(r, t)$ at $r = 0$, 10 and 20 mm on the bulk surface, respectively, which were re-plotted from figure 4. The time dependence of the magnetic pulse $B_{ex}(t)$ is also shown. In figure 5(a), the local field $B_z(t)$ near the bulk periphery starts to increase rapidly; it then decreases. On the other hand, $B_z(t)$ at the inner position rises with a time lag, decreases gradually, and approaches the final value for $t > 10$ s.

In figure 5(b), the temperature $T(t)$ near the bulk periphery starts to rise rapidly. It then decreases. The time at which the temperature starts to rise becomes delayed at the inner measuring position. At the bulk centre ($r = 0$), $T(t)$ takes a maximum at $t = 7$ s and is independent of the measuring position. It is noteworthy that the time at which $B_z(t)$ becomes maximum is about two orders of magnitude faster than the time at which $T(t)$ reaches its maximum value. These results are attributable to the lower thermal conductivity of the bulk and smaller heat transfer to the cold stage. After $B_z(t)$ reaches its maximum value, $T(t)$ becomes maximum. As a result, the local field decreases because of the flux creep. For $t > 7$ s, $B_z(t)$ becomes constant because the temperature decreases.

Figures 6(a) and (b) respectively show a simulation of the time dependence of the local field $B_z(t)$ and temperature $T(t)$ at the centre of the bulk surface ($\alpha = 4.6 \times 10^8$) after applying pulsed fields of $B_{ex} = 5$, 6 and 8 T. The peak height of $B_z(t)$

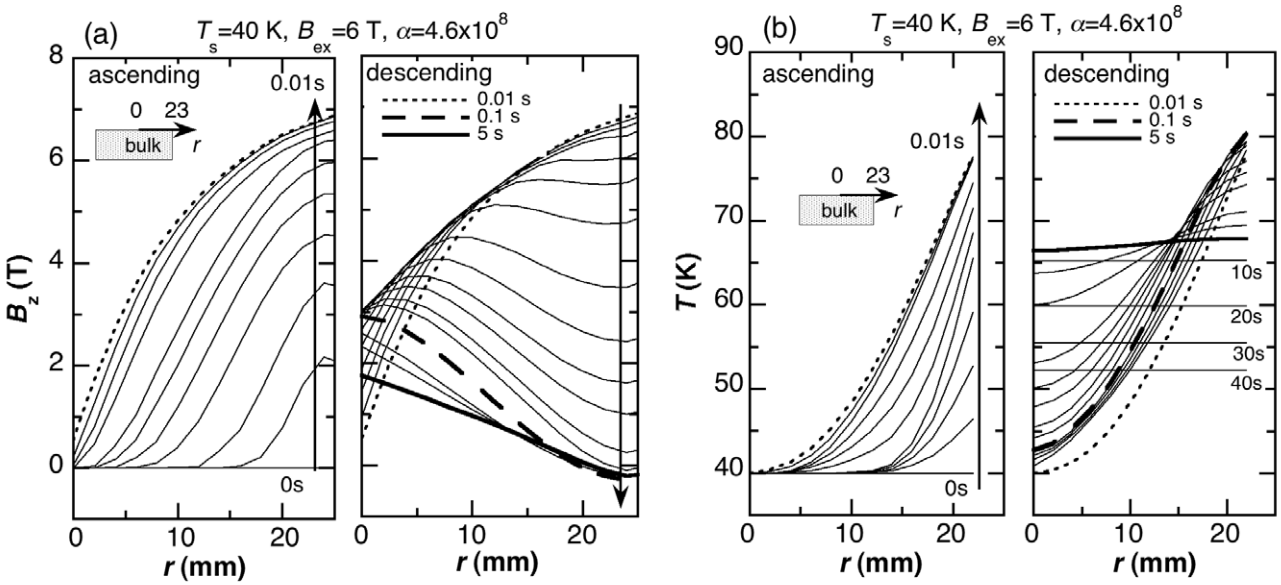

Figure 4. Time and distance dependence of (a) the local magnetic field $B(t, r)$ and (b) the temperature $T(t, r)$ on the bulk surface after applying a pulsed field of $B_{ex} = 6$ T at $T_s = 40$ K for $\alpha = 4.6 \times 10^8$. The left and right parts of each figure respectively show the ascending ($t \leqslant 0.01$ s) and descending ($t \geqslant 0.01$ s) stages.

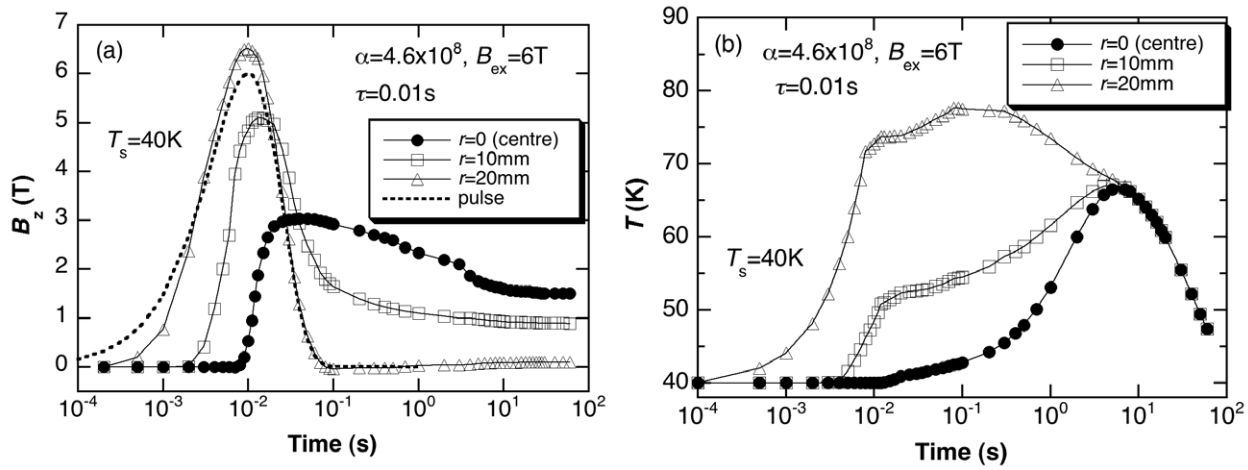

Figure 5. Time dependence of (a) the local field $B_z(t)$ and (b) the temperature $T(t)$ for $r = 0$, 10 and 20 mm on the bulk surface after applying a pulsed field of $B_{ex} = 6$ T ($\alpha = 4.6 \times 10^8$).

increases concomitantly with increasing B_{ex}. However, the time at which $B_z(t)$ takes a maximum value is about 0.05 s; it is independent of B_{ex}. In fact, $B_z(t)$ approaches the final value for $t > 10$ s. The temperature $T(t)$ increases and reaches its peak at about 7 s, which is independent of B_{ex}. The peak height of $T(t)$ increases with increasing B_{ex}.

The results of the simulation shown in figures 5 and 6 well reproduce the experimental results reported in previous papers [4, 5]. It is noteworthy that the simulation model used for this study can qualitatively demonstrate $B_z(t)$ and $T(t)$ in the bulk. However, some differences from the experimental results do exist. In the experiments at $T_s = 40$ K, the magnetic flux started to intrude and trap from 3 T at the centre of the bulk with 45 mm diameter and 15 mm thickness, which was as high-performance as $\alpha = 1.83 \times 10^9$ [4]. In existing bulks, an inhomogeneous J_c distribution exists, which arises from the crystal growth mechanism. The magnetic flux intrudes through the lower J_c paths and traps them inhomogeneously. The numerical simulation must be performed for the bulk with an inhomogeneous J_c distribution.

4.3. Application of long magnetic pulse

An extremely useful PFM technique is zero-field cooling (ZFC), of which the ascending and descending periods are of the order of 100–1000 s. Considering the Bean model, a magnetic field resembling that by FCM can be trapped by ZFC after a magnetic field twice as high as that for FCM is applied. We have reported that a trapped field B_z can be enhanced using a longer ascending magnetic pulse [12]. In

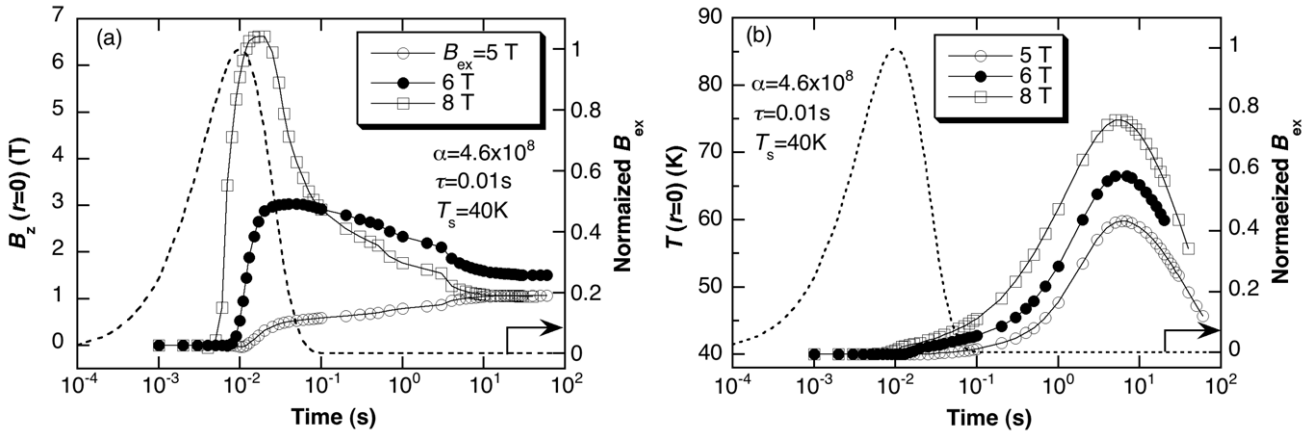

Figure 6. Time dependence of (a) the local field $B_z(t)$ and (b) the temperature $T(t)$ at the centre of the bulk surface after applying a pulsed field of $B_{ex} = 5$, 6 and 8 T ($\alpha = 4.6 \times 10^8$).

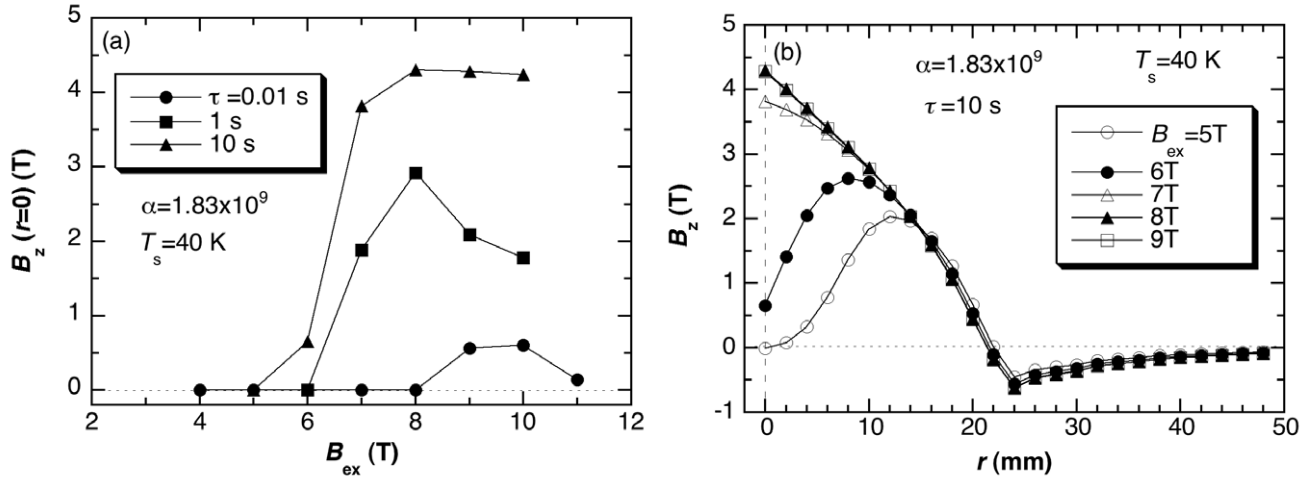

Figure 7. (a) Applied field dependence of the trapped field $B_z(r = 0)$ at the bulk centre for $\tau = 0.01$, 1 and 10 s. (b) Cross-section of the trapped field profiles for $\tau = 10$ s as a function of applied pulsed field B_{ex} ($\alpha = 1.83 \times 10^9$).

section 4.2, we presented a simulation for the bulk with lower J_c ($\alpha = 4.6 \times 10^8$; $J_{c0} = 3.3 \times 10^8$ A m^{-2} at 40 K) using a pulsed field with a rise time of $\tau = 0.01$ s. In this subsection, we present a simulation of B_z on the bulk with higher J_c ($\alpha = 1.83 \times 10^9$; $J_{c0} = 1.33 \times 10^9$ A m^{-2} at 40 K) using a longer magnetic pulse field. We discuss the origin of the B_z enhancement using a longer pulsed field and discuss the direction for the B_z enhancement using PFM.

Figure 7(a) presents the calculated trapped field $B_z(r = 0)$ on the bulk surface ($\alpha = 1.83 \times 10^9$) as a function of an applied field B_{ex} with a rise time of $\tau = 1$ and 10 s. The results for $\tau = 0.01$ s are also shown. With increasing rise time τ, the maximum trapped field $B_z(r = 0)$ increases concomitantly with increasing τ. In addition, the applied field B_{ex}^C, at which the magnetic flux starts to be trapped at the bulk centre, decreases. For example, for $\tau = 10$ s, $B_z(r = 0)$ reaches 4.3 T and B_{ex}^C decreases to 5 T. Figure 7(b) shows a typical cross-section of the trapped field profiles for $\tau = 10$ s. The $B_z(r)$ profile changes from concave to convex with increasing B_{ex} and maintains a higher B_z value. It is noteworthy that the $B_z(r = 0)$ value is enhanced for the longer τ values.

Figures 8(a) and (b) show the time evolution of local field $B_z(t)$ and temperature $T(t)$ at the centre of the bulk surface ($\alpha = 1.83 \times 10^9$) after applying a pulsed field of $B_{ex} = 8$ T with $\tau = 1$ and 10 s, respectively. In both figures, the time t_T^P at which $T(t)(r = 0)$ peaks is about 10 s, which is independent of the τ value because the thermal conductivity (κ_{ab}, κ_c) of the bulk and that of the spacing plate (κ_{cont}) are fixed. On the other hand, the time t_B^P, at which $B_z(t)(r = 0)$ peaks, increases concomitantly with increasing τ. In fact, t_B^P were, respectively 4 s and 15 s for $\tau = 1$ and 10 s. For a longer pulse application, t_B^P increases and approaches $t_T^P = 10$ s. For $\tau = 1$ s presented in figure 8(a), $B_z(t)$ decreases and saturates for $t > 10$ s, at which $T(t)$ decreases concomitantly with increasing time. The results show that the flux creep was suppressed and that a large amount of the magnetic flux remained near the bulk centre. For $\tau = 10$ s presented in figure 8(b), t_B^P is nearly equal to t_T^P; their similar behaviour is visible. This scenario is the main reason why the higher field was trapped for the long magnetic pulse application. In this regard, the long pulse application is effective for trapping a higher magnetic field. To realize a longer magnetic pulse experimentally, it is

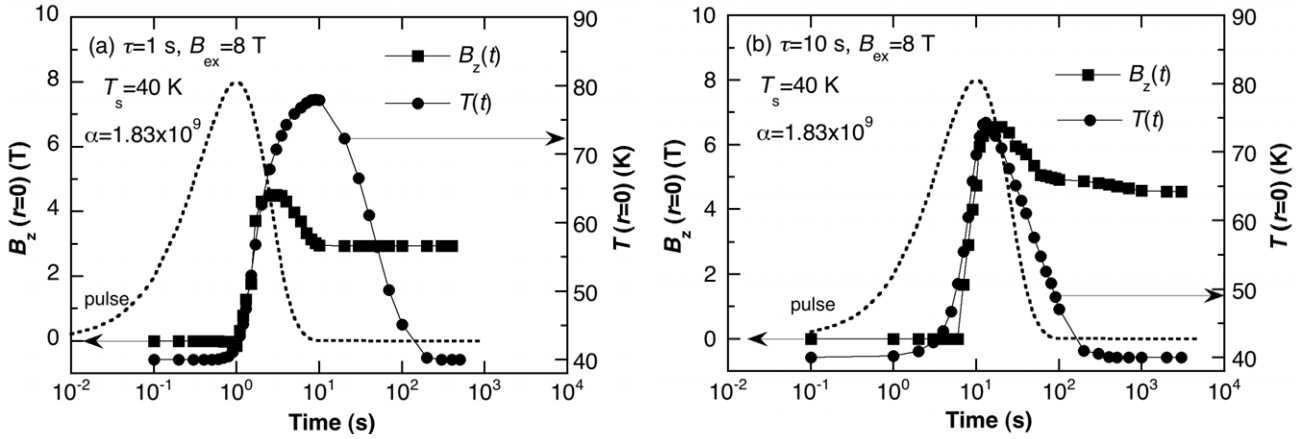

Figure 8. Time dependence of the local field $B_z(t)(r = 0)$ and temperature $T(t)(r = 0)$ for a pulsed magnetic field of $B_{ex} = 8$ T with (a) $\tau = 1$ s and (b) τ =10 s at $T_s = 40$ K. Time dependences of the applied magnetic pulse $B_{ex}(t)$ are also shown as a dotted line.

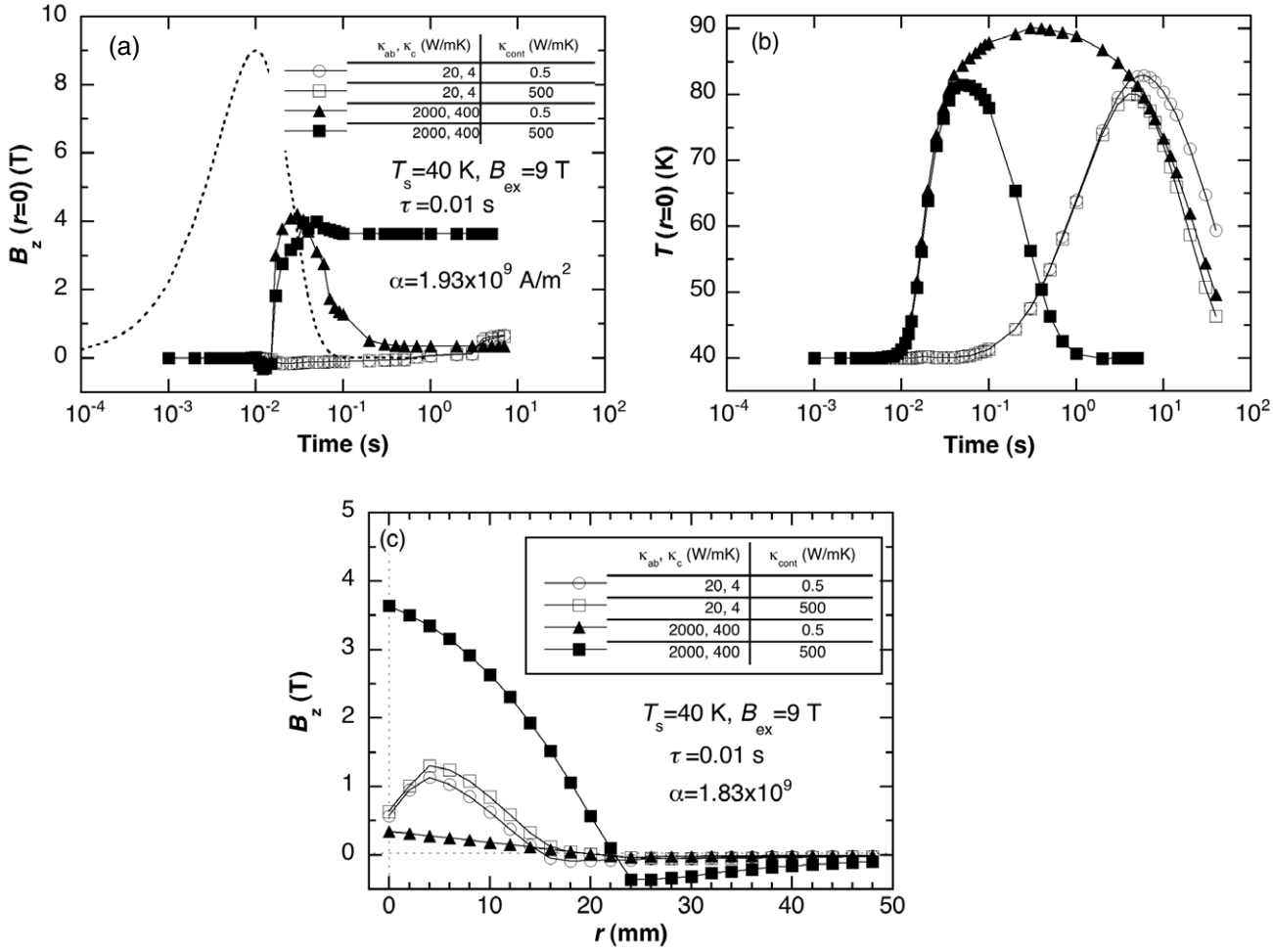

Figure 9. Time dependence of (a) the local field $B_z(t)(r = 0)$ and (b) the temperature $T(t)(r = 0)$ for a pulsed magnetic field of $B_{ex} = 9$ T with $\tau = 0.01$ s for various thermal conductivities (κ_{ab}, κ_c, κ_{cont}) ($\alpha = 1.83 \times 10^9$). (c) Trapped field profiles for respective conditions.

necessary to use a condenser bank to store a large amount of electrical energy. However, using such a device is unrealistic for practical applications at present because such condenser banks are prohibitively expensive.

4.4. Effect of thermal conductivity enhancement on the trapped field

As explained in section 4.3, a long pulsed field application is a possible solution to realize a large B_z value. However,

it is difficult to prepare a large condenser bank for a longer magnetic pulse. Using a simulation in which we can investigate an unrealistic case, exploration was performed to enhance B_z using a conventional condenser bank with $\tau = 0.01$ s. To enhance the B_z value, the time difference between t_B^P and t_T^P should be minimized. In this subsection, the effects of the thermal conductivity enhancement of the bulk and the spacing plate on the trapped field B_z are discussed.

Figures 9(a) and (b) respectively show the time evolution of a local field $B_z(t)$ and temperature $T(t)$ for the bulk with various thermal conductivities of the bulk (κ_{ab}, κ_c) and the spacing plate (κ_{cont}) after applying a pulsed field of $B_{ex} = 9$ T at 40 K. Figure 9(c) presents the trapped field profiles for each condition. For a real condition with $\kappa_{ab} = 20$, $\kappa_c = 4$ and $\kappa_{cont} = 0.5$ W mK^{-1}, the trapped field profile is shown as concave. When κ_{cont} increases to 1000 times ($\kappa_{cont} = 500$ W mK^{-1}), the trapped field does not change, although the temperature increase was reduced for $t > 10$ s. When the thermal conductivity increases to 100 times ($\kappa_{ab} = 2000$, $\kappa_c = 400$ W mK^{-1}), the generated heat diffuses over the bulk. However, the trapped field is convex but remains small because of the smaller heat transfer to the cold stage. When the thermal conductivities of both the bulk and the spacing plate increase, trapped field enhancement is predicted because the time delay between $B_z(t)$ and $T(t)$ becomes small. These results suggest that similar phenomena took place for applying a pulsed field with $\tau = 0.01$ s to those for the long pulse application ($\tau = 10$ s). However, the enhancement of the thermal conductivity for the Ag-doped bulk is as low as 10–20% [15] and enhancement of the contact thermal conductivity, i.e. enhancement of κ_{cont} cannot be realized in actual experimental set-ups.

5. Summary

A theoretical simulation of electromagnetic and thermal fields has been performed for a cryocooled superconducting bulk disc with homogeneous superconducting properties after applying a magnetic pulse. Important simulation results and conclusions obtained from this study are summarized as follows.

(1) Simulation results for bulks with various critical current densities J_{c0} qualitatively reproduced experimental results such as time and applied field dependences of the trapped field $B_z(t, r)$ and the temperature rise $T(t, r)$ on the bulk surface.

(2) For a rise time $\tau = 0.01$ s of the magnetic pulse, which is an ordinary experimental condition, the magnetic flux propagation is about two orders of magnitude faster than the heat propagation at the bulk centre because of the low thermal conductivity in the bulk. Consequently, the intruding magnetic flux escapes by the flux creep because of the delayed temperature rise.

(3) A magnetic pulse application as long as $\tau = 1$ or 10 s, which enhanced the trapped field experimentally, reduces the speed of the magnetic flux propagation. Then the difference in the propagation speed between magnetic flux and temperature becomes small. The results show that the influence on the flux creep becomes slight and the trapped field maintains a higher value. A long magnetic pulse application during PFM is a possible solution to enhance the trapped field.

(4) Based on analyses of long pulse application, we can enhance the trapped field for short pulse application through enhancement of bulk thermal conductivity and cooling power, which are two or three orders of magnitude higher than those of the real system. However, that simulation is unrealistic. Using numerical simulation, we must explore another direction to enhance the trapped field such as a multi-pulse technique for a bulk with an inhomogeneous J_c distribution.

References

[1] Yanagi Y, Itoh Y, Yoshikawa M, Oka T, Hosokawa T, Ishihara H, Ikuta H and Mizutani U 2000 *Advances in Superconductivity* vol 12 (Tokyo: Springer) p 470

[2] Sander M, Sutter U, Koch R and Klaser M 2000 *Supercond. Sci. Technol.* **13** 841

[3] Fujishiro H, Oka T, Yokoyama K, Kaneyama M and Noto K 2004 *IEEE Trans. Appl. Supercond.* **14** 1054

[4] Fujishiro H, Hiyama T, Miura T, Naito T, Nariki S, Sakai N and Hirabayashi I 2009 *IEEE Trans. Appl. Supercond.* **19** 3545

[5] Fujishiro H, Hiyama T, Tateiwa T, Yanagi Y and Oka T 2007 *Physica* C **463–465** 394

[6] Fujishiro H, Kaneyama M, Tateiwa T and Oka T 2003 *Japan. J. Appl. Phys.* **44** L1221

[7] Fujishiro H, Tateiwa T, Fujiwara A, Oka T and Hayashi H 2006 *Physica* C **445–448** 334

[8] Kajikawa K, Yokoo R, Tomachi K, Enpuku K, Funaki K, Hayashi H and Fujishiro H 2008 *Physica* C **468** 1494

[9] Komi Y, Sekino M and Ohsaki H 2009 *Physica* C **469** 1262

[10] Fujishiro H, Naito T, Furuta D and Kakehata K 2010 *Physica* C **470** 1181

[11] Fujishiro H, Kawaguchi S, Kaneyama M, Fujiwara A, Tateiwa T and Oka T 2006 *Supercond. Sci. Technol.* **19** S540

[12] Fujishiro H, Kaneyama M, Yokoyama K, Oka T and Noto K 2005 *Japan. J. Appl. Phys.* **44** 4919

[13] Kim Y B, Hempstead C F and Stand A R 1965 *Phys. Rev.* **139** A1163

[14] Ishii Y, Shimoyama J, Ogino H and Kishio K 2009 *J. Cryog. Soc. Japan* **44** 573

[15] Fujishiro H and Kohayashi S 2002 *IEEE Trans. Appl. Supercond.* **12** 1124